doi: 10.1111/j.1460-2695.2004.00804.x

A local approach to cleavage fracture in ferritic steels following warm pre-stressing

S. HADIDI-MOUD, A. MIRZAEE-SISAN, C. E. TRUMAN and D. J. SMITH

Department of Mechanical Engineering, University of Bristol, Queen's Building, University Walk, BS8 1TR, UK

Received in final form 2 April 2004

ABSTRACT Quantification of the enhancement in cleavage fracture toughness of ferritic steels following warm pre-stressing has received great interest in light of its significance in the integrity assessment of such structures as pressure vessels. A Beremin type probability distribution model, i.e., a local stress-based approach to cleavage fracture, has been developed and used for estimating cleavage fracture following prior loading (or warm pre-stressing, WPS) in two ferritic steels with different geometry configurations. Firstly, the Weibull parameters required to match the experimental scatter in lower shelf toughness of the candidate steels are identified. These parameters are then used in two- and three-dimensional finite element simulations of prior loading on the upper shelf followed by unloading and cooling to lower shelf temperatures (WPS) to determine the probability of failure. Using both isotropic hardening and kinematic hardening material models, the effect of hardening response on the predictions obtained from the suggested approach has been examined. The predictions are consistent with experimental scatter in toughness following WPS and provide a means of determining the importance of the crack tip residual stresses. We demonstrate that for our steels the crack tip residual stress is the pivotal feature in improving the fracture toughness following WPS. Predictions are compared with the available experimental data. The paper finally discusses the results in the context of the non-uniqueness of the Weibull parameters and investigates the sensitivity of predictions to the Weibull exponent, m, and the relevance of m to the stress triaxiality factor as suggested in the literature.

Keywords cleavage fracture; failure probability; local approach; residual stress; stress triaxiality; WPS.

NOMENCLATURE

a = crack length (mm)
W = ligament (mm)
a/W = crack/ligament ratio
B = specimen thickness (mm)
B_0 = reference thickness (mm)
B/B_0 = thickness correction ratio
i = order number (ascending) of a specific specimen tested in a group ($i = 1, \ldots, N$)
β = 'shape parameter' exponent for toughness-based distribution
m = Weibull exponent
N = total number of specimens tested under the same conditions (sample size)
$K_{0\mathrm{f}}$ = reference fracture toughness (MPa$\sqrt{}$m)
K_{f} = fracture toughness after WPS (MPa$\sqrt{}$m)
$K_{\min \mathrm{f}}$ = minimum (threshold) fracture toughness (MPa$\sqrt{}$m)

Correspondence: C. E. Truman. E-mail: c.e.truman@bris.ac.uk

K_{IC} = mode-I fracture toughness for the as-received conditions (MPa$\sqrt{}$m)
P_f = experimental, calibrated or predicted probability of failure (%)
T_f = triaxiality factor, maximum of the ratio of hydrostatic to von Mises stress
V_0 = reference volume in assessment of the fracture characteristic stress (mm^3)
V_p = plastic volume in calculation of Weibull characteristic stress (mm^3)
σ_f = fracture stress (average net section stress at fracture load) (MPa)
σ_{min} = minimum (threshold) characteristic reference stress (GPa)
σ_Y and σ_1 = yield stress (at specified temperature) and maximum principal stress (MPa)
σ_u = mean characteristic reference stress (GPa)
σ_w = Weibull fracture characteristic stress (GPa)
σ_h and σ_{Mises} = hydrostatic stress (mean of principals) and von Mises stress (MPa)

INTRODUCTION

The enhancement in cleavage fracture toughness of pressure vessel steels loaded at lower shelf temperatures following pre-stressing on the upper shelf and cooling (known as the warm pre-stress, WPS effect) is backed by extensive experimental evidence.[1,2] Figure 1 provides a schematic illustration of the WPS effect on toughness. However, it is not known to what extent this effect is due to localized residual stresses, crack tip blunting or a mixture of the two generated during pre-stressing. Studies by Reed and Knott[3,4] and Fowler[5] suggest that crack tip residual stresses are the dominating factor. On the other hand, Stöckl *et al*.[6] compare finite element (FE) simulations with experiments and link the WPS benefit with crack tip blunting.

Experimental observations indicate considerable uncertainty (wide scatter) in the cleavage fracture toughness of ferritic pressure vessel steels before and after warm pre-stressing.[7,8] Statistical models mostly based on Weibull three- and/or four-parameter distributions are used to describe the scatter in the test results. Examples of these expressions include K-based toughness distributions[9] as well as stress-based distributions.[10] The latter will be discussed in detail in this paper. Recent work by Smith *et al*.[11,12] also show that both K-based and/or stress-based distributions may be used to predict the WPS effect in cracked components.

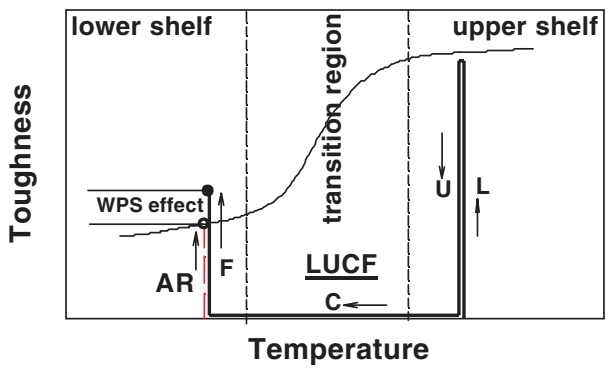

Fig. 1 Schematic description of Warm pre-stressing effect on cleavage fracture toughness.

The 'toughness-based' approach

Theoretical models using near crack tip stress and strain fields have been used to predict the WPS effect. Models describing the WPS effect, such as those developed by Curry[13] and Chell,[14] combined with a local fracture criterion as that developed by Ritchie, Knott and Rice (RKR)[15] were used by Fowler *et al*.[8] to explore scatter in the WPS effect. They used a three-parameter Wallin expression, Eq. (1), to predict the failure probability P_f of two pressure vessel steels following warm pre-stressing,

$$P_f[K_f] = 1 - \exp\left[-\frac{B}{B_0}\left(\frac{K_f - K_{min\,f}}{K_{0f} - K_{min\,f}}\right)^{\beta}\right], \quad (1)$$

where K_f represents fracture toughness after WPS. If no WPS has been applied then $K_f = K_{Ic}$, the as-received fracture toughness. Thus, Eq. (1) may be interpreted as providing the failure probability at a load corresponding to the stress intensity factor $K = K_f$ in the WPS state. The distribution parameters K_{minf} and K_{0f} were calibrated for the as-received conditions, so encapsulating the scatter in the as-received fracture toughness values, and then modified for WPS using the Chell model.[5,8] The shape parameter β was chosen by Fowler *et al*.[8] as a constant equal to 4. The ratio, B/B_0, of specimen thickness to reference length, is used to account for the thickness effect. The reference length B_0 is determined as part of the calibration procedure to the as-received toughness data.

The 'stress-based' approach

Local stress-based approaches to cleavage fracture use the Weibull distribution model as proposed by Beremin.[10,16] This method uses the Weibull parameters fitted to fracture test results from round-notched bar (RNB) specimens. In their round robin studies on micro-mechanical

models, the European Structural Integrity Society (ESIS) suggests using the parameters fitted to the RNB test results to predict cleavage fracture in pre-cracked compact tension, C(T), specimens[17] using

$$P_f[\sigma_f] = 1 - \exp\left[-\left(\frac{\sigma_w}{\sigma_u}\right)^m\right]. \quad (2)$$

In this equation, σ_f represents the net section stress at a load level that is also used to evaluate the Weibull stress, σ_w. In using the local approach the Weibull stress, σ_w, is representative of failure conditions and is determined from the following integral:

$$\sigma_w = \left[\frac{1}{V_0}\int_{V_p} \sigma_1^m \mathrm{d}V\right]^{\frac{1}{m}}. \quad (3)$$

The model is based on a weakest link theory in the form of a Weibull probability distribution, where the parameter σ_u is a reference characteristic stress corresponding to a failure probability of 63.2%, and is referred to as the mean reference stress. The Weibull exponent, m, characterizes the spread of fracture data. Further modifications to the above distribution can be made by introducing a threshold stress, σ_{min}, below which fracture is impossible and failure does not occur unless $\sigma_w > \sigma_{min}$. Equation (2) is modified so that

$$P_f[\sigma_f] = 1 - \exp\left[-\left(\frac{\sigma_w - \sigma_{min}}{\sigma_u - \sigma_{min}}\right)^m\right]. \quad (4)$$

For both distributions, shown in Eqs (2) and (4), the Weibull stress is calculated by integrating the maximum principal stress, σ_1, over a volume of the material, V, and the scale parameter V_0 is a reference volume used as a scaling factor to express σ_w in terms of stress. It is suggested that when using these distributions as a local approach to fracture, the integration volume should contain the near crack tip plastic volume, V_p.[18]

The Weibull parameters are determined from experimental results. It should be noted that in both the Beremin[10,16] and the ESIS[17] studies, the analyses were conducted assuming $\sigma_{min} = 0$. The Beremin group[10] suggests that the reference volume, V_0, is a volume equivalent to about 10 grains of the material (e.g., $V_0 = 0.001$ mm^3). This model suggests that the maximum principal stress is a characterizing parameter that determines the condition of fracture. The local approaches are also used to predict the WPS effect by Hadidimoud *et al*.[18]

Outlook of present work

In this paper, the influence of the local residual stresses arising from WPS is explored using a local approach for both pre-cracked specimens and round notched bars (RNB). A stress-based model of the probability distribution, similar to the Beremin model, is used in FE analyses together with the stress distribution under a specified loading condition at the crack tip within the plastic volume to calculate a characteristic stress, the 'Weibull stress'. This in turn is used to estimate the probability of failure corresponding to the as-received state and the loading state following warm pre-stressing. Firstly, we summarize recent experimental results that explore the influence of WPS on candidate pressure vessel steels. Then the results of FE studies incorporating analyses for local failure probability are briefly described. These results are compared with the experimental findings and discussed in relation to the influence of the crack tip residual stresses.

EXPERIMENTAL PROCEDURES AND TEST RESULTS

The experimental data presented in this section, used later to verify the predictions of the WPS effect based on the proposed model, consist of results from two types of specimens. The first series of data are those provided by current research in which shallow and sharp-notched round-notched bar, RNB, specimens of A508 steel are used. The second are test data obtained in previous test programmes[2,5,7,19] where pre-cracked compact tension, C(T), and single edge notched bend, SEN(B), specimens were used. Distributions of test results are then summarized.

A508 steel RNB test programme

Round notched bar (RNB) specimens of A508 steel were manufactured with both shallow and sharp notches. The steel used is identical to that used in earlier studies by Swankie.[19] The chemical composition and mechanical properties are summarized in Tables 1 and 2, respectively. The geometry of the RNB specimens and notch details are shown in Fig. 2. A series of tests were carried out using shallow and sharp notches with tip radii of 1.25 mm and 0.07 mm, respectively. Twenty shallow notch specimens were tested at −120 °C, 10 in the as-received condition and 10 following pre-stressing at room temperature. For the WPS tests, the pre-load level was equivalent to a net section stress of 995 MPa.

RNB tests were also carried out at −150 °C. Both shallow and sharp notched round bar specimens were tested. Shallow notched specimens contained a circumferential U-shape notch with a radius of 1.25 mm similar to those tested at −120 °C. Nine specimens were tested at −150 °C for the as-received (AR) condition and eight after warm pre-stressing (WPS). The average applied pre-load level for the WPS tests was equivalent to a net section stress of 995 MPa. The fracture stress was determined using

Table 1 Chemical analysis of A508 steel used in the experimental programme

Element	C	Si	Mn	P	S	Cr	Mo	Ni	Al	As
Weight%	0.15	0.23	1.3	0.004	0.003	0.18	0.52	0.72	0.012	0.018
Element	Co	Cu	Nb	Pb	Sn	Ti	V	W	Sb	
Weight%	0.013	0.07	<0.005	0.006	<0.005	<0.005	0.005	0.015	<0.005	

Table 2 Uniaxial tensile properties of A508 steel at test temperatures

Orientation	Temperature	E (GPa)	ν	σ_{yield}
L	20	200	0.3	430
T	−120	200	0.3	632
L,S	−150	200	0.3	696

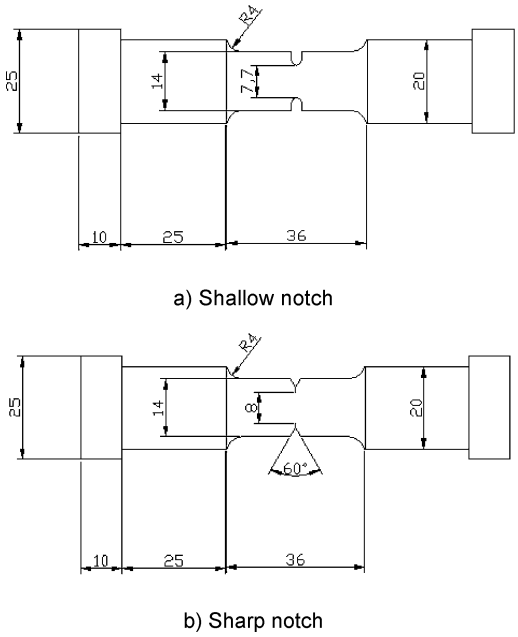

Fig. 2 Geometry and orientation for shallow and sharp notch A508 steel RNB specimens (all dimensions in millimetre).

the applied load divided by the measured final net section area.

Sharp notches were introduced into 17 specimens by the electro discharge machining (EDM) technique. Circumferencial notches with a tip diameter between 0.05 and 0.07 mm were obtained. Ten specimens were tested in the as-received condition at −150 °C and the remaining specimens were fractured at −150 °C following pre-loading to an equivalent average stress of 935 MPa at room temperature. All of these specimens failed by cleavage.

Scanning electron microscopy (SEM) was used to observe the details of the fracture surfaces. Details of typical fracture surfaces suggested that the specimens tested at −150 °C and −120 °C had failed purely by cleavage and predominantly by cleavage fracture, respectively. In fact, only the shallow notched specimens displayed shear lips at −120 °C. Typical observations are shown in Fig. 3. The fracture surface in Fig. 3a belongs to a shallow notched specimen tested at −120 °C with indication of shear lips near the root of the notch and final cleavage fracture across the remainder of the section. The detailed section shown in Fig. 3b demonstrates strong evidence of cleavage failure at −150 °C for both shallow and sharp notch specimens throughout the section.

Test results from other experimental programmes

A533B pressure vessel steel was used in earlier test programmes by Smith and Garwood,[2,7] Fowler,[5] Fowler *et al*.[8] and Swankie.[19] The test results were summarized and used to study the WPS effect by Smith *et al*.[11,12] For the A533B steel, tests were carried out by Smith and Garwood[7] using single edge notch bend (SEN(B)) specimens containing fatigue pre-cracks with nominal crack length to width ratio, $a/W = 0.5$. Fourteen specimens in the as-received conditions were fractured at −170 °C with another fourteen pre-loaded and unloaded at room temperature and then cooled and fractured at −170 °C (the LUCF loading cycle). The pre-loading level was equivalent to an elastic stress intensity factor of 120 MPa$\sqrt{}$m. All tests at low temperature failed in a brittle manner by cleavage fracture.

Summary of experimental results

Table 3 shows a summary of the experiments used in this work. In all tests the failure probability was determined from[20]

$$P_f = \frac{i - 0.5}{N}, \tag{5}$$

where N and i are the total number of specimens and the order number, respectively.

Fracture stress results (i.e., average net section stress) obtained from tests of A508 steel RNB specimens are summarized in Fig. 4. Shallow-notched specimens tested at −120 °C are shown in Fig. 4a while Figs 4b and c present the results for specimens fractured at −150 °C for shallow and sharp notches, respectively. Unlike the sharp notch RNB test data, the experimental results from the shallow

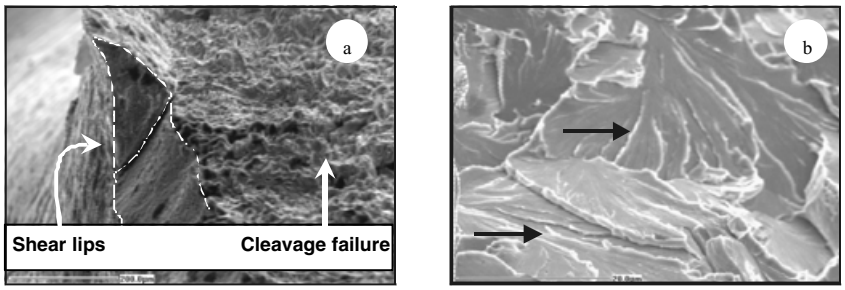

Fig. 3 Fracture surfaces at the notch section for A508 steel RNB specimens. (a) Evidence of shear slips at −120 °C. (b) Indication of cleavage fracture at −150 °C.

Table 3 Summary of test configurations

Material	Specimen	Test temperature (°C)	Test condition	Sample size
A508	RNB (shallow)	−120	AR/WPS	10/10
A508	RNB (shallow)	−150	AR/WPS	9/8
A508	RNB (sharp)	−150	AR/WPS	9/8
A533B	SEN(B)–50 mm	−170	AR/WPS	14/14

notched RNB tests show far less improvement following warm pre-stressing. Rather the beneficial influence of WPS appears to be limited in RNB specimens and yet only at lower levels of failure stress. The reason for this contrast between the pre-cracked specimens and the notched-RNB specimens is explored later.

The fracture test results for A533B steel summarized in the previous section were directly interpreted in terms of failure probability against fracture toughness, with the failure probability P_f determined using Eq. (5). The fracture toughness (or stress intensity at fracture) was determined from the maximum load at fracture and the assumed crack lengths. The results are shown in Fig. 5. The experimental results from the pre-cracked C(T) and SENB specimens demonstrate that there is a considerable improvement in fracture toughness following WPS as shown in Fig. 5 for A533B steel.

FINITE ELEMENT STUDIES

Finite element models

Throughout the numerical FE studies, meshes were created in ABAQUS/CAE and then the analysis performed using the ABAQUS finite element code.[21] For the pre-cracked compact tension, C(T), specimens two- and three-dimensional FE models with a refined mesh around the crack tip were created. Due to symmetry only one half of the specimen was modelled for two-dimensional analysis and one quarter for the three-dimensional analysis. Eight node quadratic elements with reduced integration were used for plane strain two-dimensional models where the element size at the crack tip was 0.05 mm. Three-dimensional models used eight-node elements with reduced integration (C3D8R) with similar mesh refinement ahead of the crack tip and a larger element size in the thickness direction. For the pre-cracked SEN(B) specimens, only three-dimensional FE models were created with similar features to the C(T) three-dimensional model. Only three-dimensional model simulation results were used in the model assessments. For the model of the RNB specimen axial symmetry allowed the use of axi-symmetric elements (iso-parametric quadratic eight-node with reduced integration) and due to the plane of symmetry across the section at the notch, only one half of the specimen was modelled. The smallest element size was approximately 0.15 mm. For the assessment of the proposed model, both materials post yield response were considered as isotropic hardening. However, a kinematic hardening elastic–plastic material law was also used to examine the effect of the hardening law on the fracture toughness predictions. This is detailed later. For A533B steel, the yield strengths (0.2% offset) are 530 MPa and 893 MPa at 20 °C and −170 °C, respectively. Finally, for A508 steel, the yield strengths are 430 MPa at 20 °C, 632 MPa at −120 °C and 696.0 MPa at −150 °C. Detailed material data for the A508 steel is provided by Carassou.[22]

To estimate the probability of fracture based on Eqs (3) and (4), a routine ('Local') was written to perform the analysis using the results from the FE simulations. The

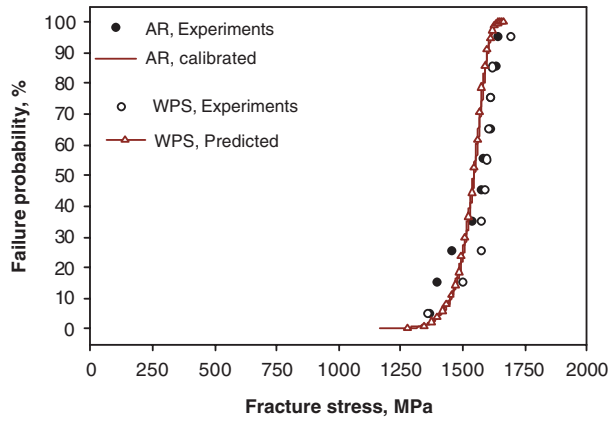

a) Shallow notch at -120°C

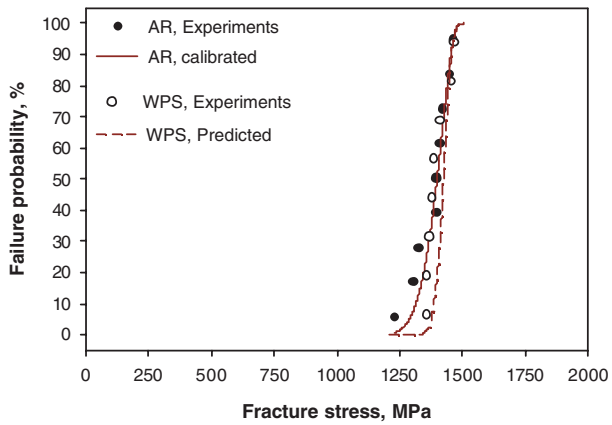

b) Shallow notch at -150°C

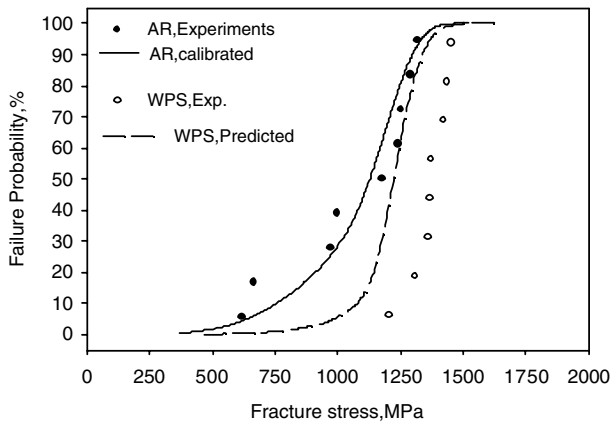

c) sharp notch at -150°C

Fig. 4 Distribution of fracture-test data for as-received and WPS tests for A508 steel RNB specimens. (a) Shallow notch at −120 °C (b) shallow notch at −150 °C and (c) sharp notch at −150°C.

integration volume was chosen such that the region (elements) where plastic straining took place was included in the calculation of probability and σ_1, the maximum principal stress, was used to calculate the Weibull stress. Elements at the boundary of the plastic region were also included if integration points within the elements exceeded the yield strength. The procedure for determining the probability of failure was repeated for each load increment in the FE analysis. To ensure that the plastic volume was included completely in the integration process, required for calculation of the Weibull stress, all elements in the model were checked for plasticity.

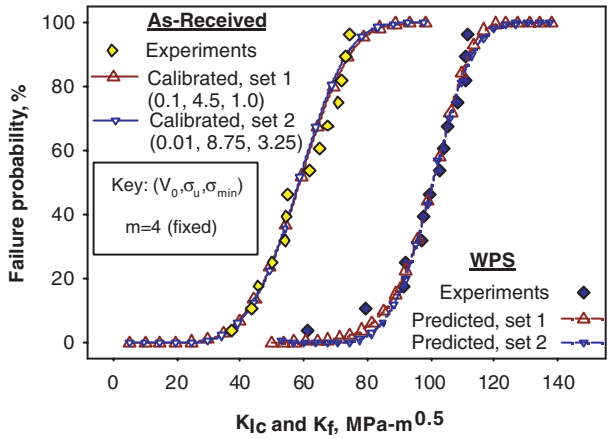

Fig. 5 Distribution of test data for as-received and prediction of WPS effect for A533B steel SEN(B) specimens at −170 °C with calibrate three-dimensional Weibull parameters.

To implement Eqs (3) and (4), details of four Weibull parameters (m, V_0, σ_u and σ_{min}) were required. The procedure for determining these parameters is described in the next section and later we describe results obtained from simulating WPS conditions.

Calibration of Weibull parameters

The calibration process for the determination of the Weibull parameters using the fracture toughness test data has been also studied by Gao and co-workers.[22,23] Their results demonstrate that the four parameters (m, V_0, σ_u and σ_{min}) cannot be uniquely defined. They set V_0 equal to 1 and calibrate the other parameters using test data for two different levels of constraint. The shape parameter m has also been shown by Milella and Bonora[24] to be a function of the notch tip geometry (or alternatively local triaxial stress-state). For blunt notches in ferritic steels m is in the range of 20 or higher while it decreases to approximately four for sharp cracks. For pre-cracked specimens, and to maintain consistency between Eqs (1) and (3), we select $m = \beta = 4$ and calibrate the remaining parameters using the fracture toughness results for the as-received tests shown in Fig. 5. Throughout the FE calibration studies it was assumed that the materials exhibited isotropic hardening. The effect of material hardening on the predictions is presented later.

The Weibull stress (σ_w) is a function of V_0 and m and for a given value of V_0 the remaining parameters (σ_u and σ_{min}) were determined by obtaining failure probabilities from the three-dimensional FE analysis that visually best matched the experimental as-received data for A533B steel. The distribution parameters were non-unique and two sets (1 and 2) of the Weibull parameters, σ_u and σ_{min}, were obtained for two values of V_0. The results of the three-dimensional calibration study are illustrated in Fig. 5 where the estimated probability of failure is shown for the two sets of parameters. For set 1, with $V_0 = 0.01$ mm^3, the calibrated values of σ_u and σ_{min} are 8.75 GPa and 3.25 GPa, respectively. Similarly for set 2, with $V_0 = 0.1$ mm^3, $\sigma_u = 4.5$ GPa and $\sigma_{min} = 1$ GPa also provided an excellent estimate of failure probability, almost identical to those obtained from set 1. As shown, the two sets of parameters result in very similar distributions for both the as-received and WPS tests.

For the A508 steel RNB tests, the as-received data were used to calibrate the Weibull parameters. The four Weibull parameters in the distribution function are interdependent and thus one has to be pre-selected for the calibration process. Unlike the analysis for the pre-cracked data, V_0, was arbitrarily fixed to be 0.001 mm^3 while m was considered a free parameter. An initial estimate for the exponent, $m = 23$, was taken from earlier analyses[17] and then the distribution parameters were calibrated for A508 steel using as-received data using the same procedure described for the cracked specimens. The parameter values that provided the best agreement with the as-received experimental results for the shallow notch tests at -120 °C are $m = 23$, $\sigma_u = 2.78$ GPa and $\sigma_{min} = 0$ GPa. The calibrated parameters for the shallow notch tests at -150 °C are $m = 24$, $\sigma_u = 3.16$ GPa and $\sigma_{min} = 0.8$ GPa. Similar procedures were followed to determine the parameters that best matched the as-received data for sharp notch RNB tests at -150 °C. The calibrated parameters are $m = 8.0$, $\sigma_u = 4.98$ GPa and $\sigma_{min} = 0.0$ GPa. Using these values the estimated curves for probability of fracture for the RNB tests with shallow notches tested at -120 °C and -150 °C are shown in Figs 4a–c. The calibrated Weibull parameters are summarized in Table 4.

Simulation of WPS

The calibrated sets of Weibull parameters for different specimen configurations and test temperatures were then used to predict the enhancement in cleavage fracture toughness following the LUCF cycle for both pre-cracked SEN(B) and RNB specimens. Pre-loading and unloading at room temperature was simulated using elastic–plastic material properties at room temperature. The material properties were then transformed from room temperature values to their low-temperature values. This was accomplished in one step of the analysis during which the residual stress field was allowed to redistribute and adjust prior to reloading to fracture at a low temperature. The simulation was then continued using the elastic–plastic mechanical properties at the lower fracture temperature. The probability of failure was determined using the 'Local' subroutine together with the calibrated Weibull parameters from the as-received fracture behaviour described above. It should be noted that the 'Local' subroutine was used to determine P_f only during the final reloading at low temperature and not during the prior loading and unloading at room temperature. Also, no changes to the Weibull parameters were made as a result of prior loading. On reloading to fracture at low temperature the stress field in the newly developing plastic zone will be different from the as-received tests. This effect is presented later. A key feature in the 'Local' analysis following WPS was to identify the 'active' plastic volume. The initial plastic zone (arising from WPS) was assumed not to be reactivated until the plastic strain on reloading exceeded the plastic strain arising from WPS.

FINITE ELEMENT RESULTS

Probability of failure

The results from the WPS simulations for A508 steel RNB specimens with shallow notches at -120 °C and -150 °C are shown in Figs 4a and b, respectively. Predictions compare well with the experimental results and notably at -120 °C. The simulations illustrate that there is no change in fracture stress after WPS. In contrast,

Table 4 Summary of calibrated Weibull parameters based on as-received test data

Material	Specimen	Temperature (°C)	V_0 (mm^3)	M	σ_u (GPa)	σ_{min} (GPa)
A508	RNB (shallow)	−120	0.001	23	2.78	0.0
A508	RNB (shallow)	−150	0.001	24	3.16	0.8
A508	RNB (sharp)	−150	0.001	8	4.98	0.0
A533B	SEN(B)-50 mm	−170	0.01	4	8.75	3.25
			0.10	4	4.5	1.0

for shallow notch tests at −150 °C the model predicted a shift in fracture stress corresponding to lower experimental fracture stresses and yet for higher fracture stresses predicted no improvement as suggested by the experimental data. In both cases, significant plasticity occurred prior to fracture that resulted in much less improvement, if any, especially for high fracture loads. Predicted failure probabilities after WPS for sharp-notched RNB tests at −150 °C, shown in Fig. 4c, illustrate less improvement in fracture stress compared to the experimental data.

For the pre-cracked SEN(B) A533B specimens two sets of Weibull parameters, shown in Fig. 5, were used to predict failure of probability following WPS using three-dimensional analyses. The resulting predictions for WPS are shown in Fig. 5 for A533B. Significant improvement in toughness following WPS is predicted, consistent with the experimental results. It is apparent that both sets (1 and 2) of Weibull parameters provide essentially identical predictions of the WPS effect illustrating that the Weibull parameters are non-unique. The Weibull characteristic stress evaluation is affected by mesh refinement, the region included in the plastic volume in calculation of the integral, and more importantly the through thickness stress distribution. These parameters explain the difference in two-dimensional and three-dimensional model predictions as seen in Fig. 6a. The differences between two-dimensional and three-dimensional predictions are consistent with the corresponding AR fits.

The effect of the hardening response of the material in the predictions was also examined by applying the predictive approach for a specific configuration with both isotropic and kinematic hardening models. Firstly, the isotropic hardening model was used in conjunction with the FE analysis simulating the as-received conditions to estimate calibration parameters that provided a close fit to the experimental data. The same parameters were then used in a second analysis using a kinematic hardening material model. The predicted as-received distribution was virtually the same as that calibrated based on isotropic hardening material data. Furthermore, the calibrated parameters were used in the WPS simulations using both hardening models. Very similar results with good agreement to the experimental WPS data were obtained. It was therefore concluded that the hardening effect with regard to the WPS effect was quite marginal. Results are shown in Fig. 6b.

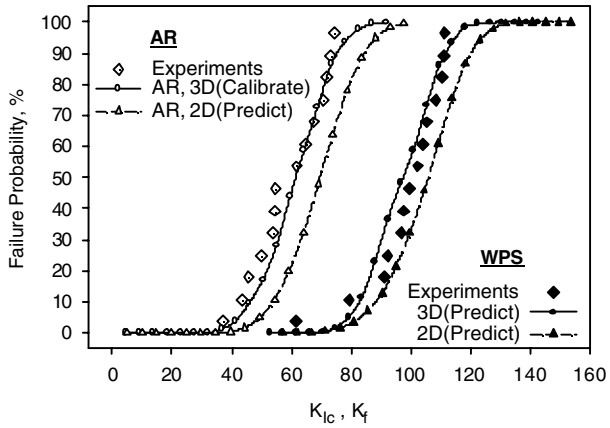

a) 2-D and 3-D model predictions

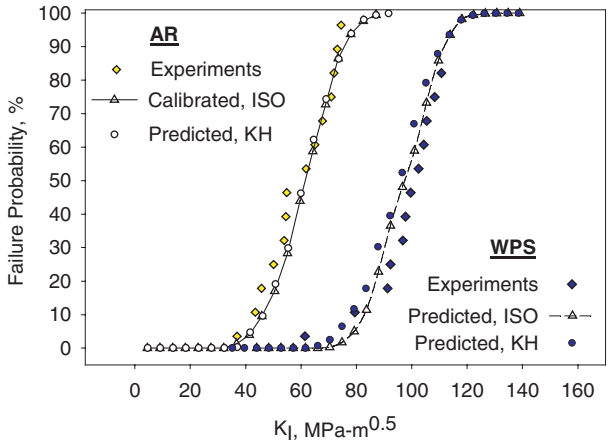

b) The effect of material hardening on the local approach predictions
ISO=isotropic Hardening, KH=Kinematic Hardening

Fig. 6 Comparison of experimental results with finite element simulations for as-received and WPS condition for A533B steel at −170 °C. (a) Two- and three-dimensional model predictions. (b) The effect of material hardening on the local approach predictions.

Local crack tip stresses

The stress distribution along the crack line of fracture specimens, or across the section in the case of RNB specimens, is affected by warm pre-stressing. This is due to the presence of the initial stress field (i.e., residual stresses), especially in the vicinity of the crack tip, resulting from plastic deformation induced through pre-loading. This does not exist in the case of as-received conditions. An understanding can be gained of the influence of WPS by examining the notch and near crack tip stresses. Figure 7 shows the distributions of the normal stress, σ_{yy}, at the onset of brittle failure in the RNB, with (a) shallow notch, (b) sharp notch and (c) fracture specimens. For the pre-cracked SENB or C(T) specimens, the stress distribution corresponds to a combined elastic–plastic state ahead of the crack tip. In contrast to the RNB specimens there is much more widespread plasticity and in particular for shallow notched RNB specimens, analysis indicates that the stress distribution is associated with a fully plastic state across the net section. Also shown in Fig. 7 are the stress distributions at lower load-levels.

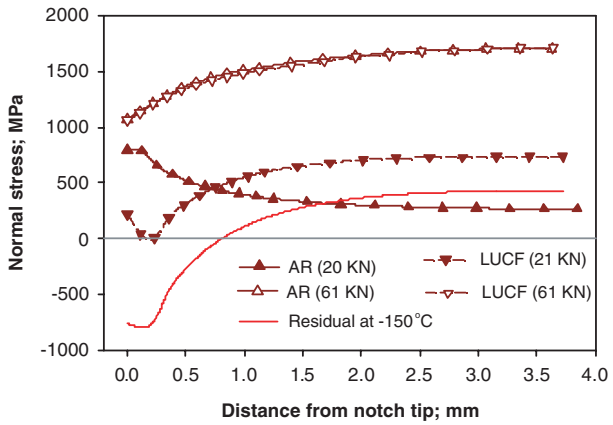

a) A508 steel RN(B) at -150C with shallow notch

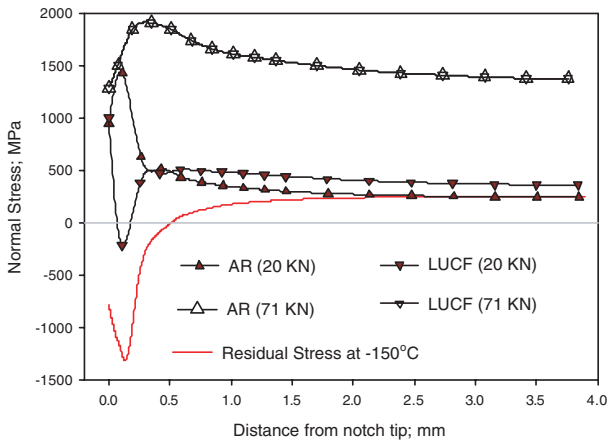

b) A508 steel RN(B) at -150C with sharp notch

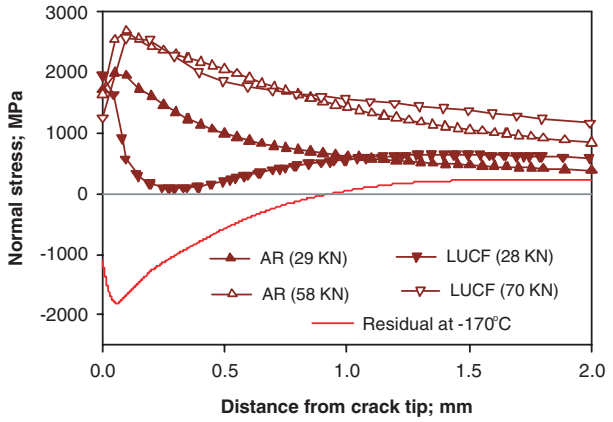

c) A533B steel C(T) model at -170C

Fig. 7 Normal to the crack line stress distributions near the crack tip for as-received and WPS conditions (a) A508 steel RN(B) at −150 °C with shallow and (b) sharp notch (c) A533B steel C(T) model at −170 °C.

Using the results of FE simulations for warm prestressing residual stress distributions ahead of the crack and notch tips were obtained as shown in Figs 7a–c as functions of the distance from the crack tip. Results show that a compressive residual stress field extends to distances ahead of the crack and notch tip of about 1 mm. On reloading at lower temperatures, the local residual stress field combined with the stress field induced by the applied loading is lower than the stress field associated with applied loading alone. This is particularly true near the crack and notch tips. Further away, the combined stress is greater than that for applied loading alone. For the pre-cracked C(T) specimen a greater applied load (i.e., 70 kN in the case of A533B at −170 °C) is required after WPS to match the stress distribution for the failure load (i.e., 58 kN for the same steel/temperature) in the as-received state (Fig. 7c). A similar argument applies to the RNB tests with a sharp notch fractured at −150 °C (Fig. 7b). In contrast, for the RNB specimen with a shallow notch at an applied load (61 kN) after WPS, equal to the applied load for failure in the as-received state, the stress distribution ahead of the notch tip is essentially the same as that without WPS (Fig. 7a). There is little or no influence of the residual stress field following WPS for the RNB with a shallow notch particularly at higher fracture loads.

Role of stress triaxiality

One possible route to include the role of constraint in the failure prediction model is to correlate the stress triaxiality factor, T_f, with the Weibull exponent, m. Milella and Bonora[24] investigated this issue. In their study T_f, the ratio of hydrostatic stress to Mises stress was plotted against the calibrated Weibull exponent, m, determined at the fracture load. Calibration of m was based on the as-received fracture data for a wide range of fracture test configurations as well as RNB s with various notch tip radii. T_f was defined by Eq. (6),

$$T_f = \mathrm{Max}(\sigma_h/\sigma_{\mathrm{Mises}}), \tag{6}$$

as the maximum of the ratio of hydrostatic to von Mises stress within the plastic volume. They suggested that the exponent m, which influences the slope of the distribution of fracture data, can be related to T_f as

$$m = 55.4 - 22.4\,(T_f). \tag{7}$$

To investigate the suggested linear relationship between the two parameters, the stress results obtained from FE analyses were used to determine T_f for the various configurations studied in this work. In cases where the model predictions are consistent with the experimental data, m–T_f pairs shown in Fig. 8 appear very close to the empirical Milella–Bonora line, whereas for the sharp notch RNB model this is not the case. For example, a value of $m = 4$ suggested in the local approach for crack is lower than the value corresponding to its triaxiality factor on the empirical line. It can be seen that T_f values for as-received and

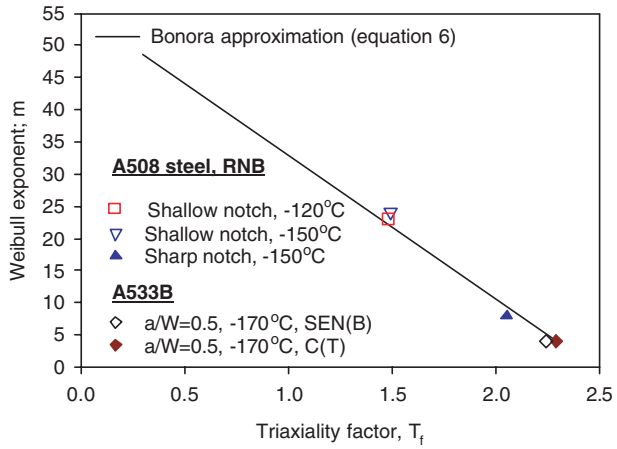

Fig. 8 Weibull exponent plotted against stress triaxiality factors corresponding to various configurations compared with the empirical relationship suggested by Milella and Bonora.

WPS conditions of the same test configuration are generally very similar, while for sharp notch RNB the distribution of experimental data are in favour of higher m values for the WPS results as compared with the as-received data.

DISCUSSION

The local approach presented here is based on a weakest link theory and assumes that should the maximum principal stress reach a critical level sufficient to activate any crack initiator, failure will occur. Stress distributions described for different types of cracked specimens fractured in both the as-received and the warm pre-stressed conditions suggest that at the fracture load the maximum principal stress attained its maximum value very close to the crack tip. The local approach is associated with the maximum principal stress within a localized plastic volume at the crack tip. The crack tip region is also where, in the case of WPS conditions, the residual stress field generated on pre-loading and unloading mostly suppresses stresses on reloading and thus acquires a higher level of fracture load or 'apparent toughness'. The distribution of normal (to the crack plane) stress from the as-received and WPS analyses, shown in Fig. 7c, supports this argument. The level of enhancement in cleavage fracture toughness, however, depends on how dominantly the maximum principal stress characterizes the onset of failure. In other words, this depends on how descriptive this stress component is of the failure conditions and whether and how other stress components may contribute to the occurrence of cleavage fracture.

Application of a local approach that uses maximum principal stress within the plastic volume as a failure criterion to RNB specimens showed less improvement in toughness after WPS than seen in the experiments. On the other hand, the extent of plasticity at failure for these cases is rather high compared with the high constraint geometries such as C(T) or SEN(B). The normal stress distributions across the section of shallow and sharp notch RNB specimens are shown in Figs 7a and b. It can be concluded that the local stress-based approach in the form presented is applicable to high constraint problems only, whereas further modifications may be required to validate the suggested predictive model for the effect of WPS on low constraint problems.

For shallow notch tests the maximum principal stress has its maximum value at the centre of the cross section, and not at the notch tip, as shown in Fig. 7a. Thus, according to the above discussion, it is not expected for WPS to influence the conditions of failure especially at higher fracture loads where plasticity is contained throughout the section. Experimental data and model predictions consistently support this conclusion.

Under-predicted failure probabilities shown in Fig. 4c for sharp notch RNB strengthen the argument that further modifications to the local approach are necessary. As mentioned earlier, for RNB specimens the fracture condition is associated with significant plastic deformation of much larger extent than the highly constrained fracture specimens. Furthermore, the degree of crack tip-blunting upon loading and unloading at room temperature is much higher for these specimens than the highly constrained fracture specimens. This also suggests using higher values of m for the case of low constraint geometries.

The empirical linear relationship between the Weibull exponent and the triaxiality factor exhibits a sharp slope suggesting that the value of m is sensitive to changes in triaxiality factor

$$\delta m = -22.4 \times \delta\,(T_f)\,. \tag{8}$$

The shape of the scatter in the fracture toughness results (i.e. the failure distribution function) is very sensitive to the value of the exponent m, especially for lower values characterizing cracks and sharp notches. A very accurate estimation of triaxiality factor, which is not easy to obtain, is thus required to achieve an appropriate modification of m. Extreme caution must be exercised when using this relation to modify m in the presence of sharp cracks.

Empirical curve fitting of the experimental results of sharp notched RNB tests revealed that the shape parameter changed from about 5 (fitted to the as-received data) to 11 (more appropriate to predict WPS data). This indicates that following WPS the toughness distribution becomes narrower. This is evident from the results shown in Fig. 4c. However in the FE analysis the shape parameter m for the local analysis of the pre-cracked specimen was selected to be equal to 4 for the as-received state, while following

WPS we assumed that m remained unchanged (Fig. 5). The assumption that m remains unchanged appears to be appropriate for the shallow notched RNB simulations (with $m = 24$) as for high values of m the failure distribution is not sensitive to its value but this is not always the case for the pre-cracked simulations. In the former case, an improvement in toughness is obtained at low fracture loads because of the presence of residual stress. At higher loads and for conditions corresponding to wide spread plasticity, the influence of the residual stress is negligible. This is because the residual stresses are completely wiped out through plastic deformation which is similar to the argument given by Curry.[13]

CONCLUDING REMARKS

The local approach has the advantage of using the same set of parameters for both the as-received and warm pre-stressed conditions at least for high constraint fracture problems.

This work and others[23,24] demonstrate that the parameters required to predict the probability of failure using the local stress-based approach are not unique. In earlier work by Gao *et al*.[23] it was suggested that better estimates of the Weibull parameters would be attained from two data sets corresponding to two different levels of 'constraint'. This is the same as having two sets of specimens with different local stress distributions. The introduction of a crack tip residual stress field in pre-cracked specimens using WPS also provides a different local stress field. Here we have not used the approach developed by Gao *et al*.[23] and Ruggieri *et al*.[24] Rather we provide a calibrated set of Weibull parameters using only the as-received data and then use the same parameters to predict the effects of WPS for the LUCF cycle.

Investigation of the role of the material hardening response on the predictions obtained from the local stress-based approach to cleavage fracture suggested no influence on the distribution or on the predicted WPS effect.

Earlier work by Millela[25] showed that the shape parameter was a function of local triaxial stress-state with m increasing with decreasing triaxiality factor. The presence of residual stress and crack tip blunting after WPS alters the triaxiality. The results presented in this work appear to be consistent with this suggestion as shown in Fig. 8 although this issue will require further investigation.

Acknowledgements

This work was supported by EPSRC grant GR/N10714 in collaboration with TWI Ltd. Their support is fully appreciated. The authors would like to thank their co-workers at TWI and the industrial partners for their advice during the course of the work. The first author would also like to thank Ferdowsi University of Mashhad, Iran, for granting him permission to participate in this work.

REFERENCES

1 Pickles, B. W. and Cowen, A. (1983) A review of warm pre-stressing studies. *Int. J. Press. Vessel Pip.* **14**, 95–131.
2 Smith, D. J. and Garwood, S. J. (1990) The significance of prior overload on fracture resistance—a critical review. *Int. J. Press. Vessel Pip.* **41**, 255–296.
3 Reed, P. A. S. and Knott, J. F. (1996) Investigation of the role of residual stress in the warm pre-stress (WPS) effect: part I—experimental. *Fatigue Fract. Engng Mater. Struct.* **19**, 485–500.
4 Reed, P. A. S. and Knott, J. F. (1996) Investigation of the role of residual stress in the warm pre-stress (WPS) effect: part II—analysis. *Fatigue Fract. Engng Mater. Struct*. **19**, 501–513.
5 Fowler, H. (1998) The influence of warm pre-stressing and proof loading on the cleavage fracture toughness of ferritic steels. Ph.D. thesis, University of Bristol, UK.
6 Stöckl, H., Böschen, R., Schmitt, W., Varfolomeyev, I. and Chen, J. H. (2000) Quantification of the warm pre-stressing effect in a shape welded 10 MnMoNi 5-5 material. *Engng Fract. Mech*. **67**, 119–137.
7 Smith, D. J. and Garwood, S. J. (1990) Experimental study of effects of prior overload on fracture toughness of A533B steel. *Int. J. Press. Vessel Pip*. **41**, 297–331.
8 Fowler, H., Smith, D. J. and Bell, K. (1997) Scatter in cleavage fracture toughness following proof loading. In: Advances in fracture research. In: Proceedings of 9th International Conference Fracture (ICF 9). **Vol. 5**, pp. 2519–2526.
9 Wallin, K. (1991) Statistical modelling of fracture in the ductile-to-brittle transition region. In: *Defect Assessment in Components, Fundamentals and Applications* (Edited by J. G. Blauel, K. H. Schwalbe). ESIS/EGF 9, Mechanical Engineering Publications, London, pp. 415–445.
10 Beremin, F. M. (1983) A local criterion for cleavage fracture of a nuclear pressure vessel steel. *J. Metall. Trans*. **14A**, 2277–2287.
11 Smith, D. J., Hadidimoud, S. and Fowler, H. (2003) The effects of warm pre-stressing on cleavage fracture: part 1—evaluation of experiments. *Engng Fract. Mech*. (corrected copy submitted).
12 Smith, D. J., Hadidimoud, S. and Fowler, H. (2003) The effects of warm pre-stressing on cleavage fracture: part 2—finite element analysis. *Engng Fract. Mech*. (corrected copy submitted).
13 Curry, D. A. (1981) A micro-mechanistic approach to the warm pre-stressing of ferritic steels. *Int. J. Fract*. **17**, 335–343.
14 Chell, G. G. (1980) Some fracture mechanics applications of warm pre-stressing to pressure vessels. In: *Proceedings of 4th International Conference Pressure and Vessels*. Technology, IMechE, pp. 117–124.
15 Ritchie, R. O., Knott, J. F. and Rice, J. R. (1973) On the relationship between critical tensile stress and fracture toughness in mild steel. *J. Mech. Phys. Solids* **21**, 395–410.
16 Beremin, F. M. (1981) Numerical modelling of warm pre-stress effect using a damage function for cleavage fracture. Proceedings of 5th international Conference on Fracture, ICF5, **Vol. 2**, Oxford Pergamon.
17 Catherine, C. S. and Poussard, C. (2000) Prediction of cleavage toughness on CT specimen. Numerical Round Robin on Micro-Mechanical Models. ESIS TC 8.

18 Hadidimoud, S., Mirzaee-Sisan, A., Truman, C. E. and Smith, D. J. (2002) Predicting how crack tip residual stresses influence brittle fracture. ASME Pressure Vessels and Piping Conference (PVP2002), Vancouver, Canada, **Vol. 434**, pp. 111–116.
19 Swankie, T. D. (1999) The role of shear and constraint in mixed mode fracture. Ph.D. thesis, University of Bristol, UK.
20 Bergman, B. (1984) On the estimation of Weibull modulus. *J. Mater. Sci. Lett.* **3**, 689–692.
21 Hibbit, K. and Sorenson, Inc. (2001) ABAQUS Users Manuals (Version 6.2), HKS Inc., 1080 Main Street, Pawtucket, RI 02680–4847, USA.
22 Carssou, S. (1999) Delenchement du clivage dans un acier faiblement allie: role de l'endommagement ductile localise autour des inclusions ≫, Ph.D. thesis, Ecole des Mines de Paris, France.
23 Gao, X., Ruggieri, C. and Dodds, R. H. (1998) Calibration of Weibull stress parameters using fracture toughness data. *Int. J. Fract*. **92**, 175–200.
24 Ruggieri, C., Gao, X. and Dodds R. H. (2000) Transferability of elastic-plastic fracture toughness using the Weibull stress approach: Significance of parameter calibration. *Engng Fract. Mech*. **67**, 101–117.
25 Milella, P. P. and Bonora, N. (2000) On the dependence of the Weibull exponent on geometry and loading conditions and its implications on the fracture toughness probability curve using a local criterion. *Int. J. Fract*. **104**, 71–87.